PNAS RESEARCH ARTICLE | MEDICAL SCIENCES

Hypersensitivity to ferroptosis in chromophobe RCC is mediated by a glutathione metabolic dependency and cystine import via solute carrier family 7 member 11

Long Zhang[a], Charbel S. Hobeika[a], Damir Khabibullin[a], Deyang Yu[b,c,d], Harilaos Filippakis[a], Michel Alchoueiry[a], Yan Tang[a], Hilaire C. Lam[a], Peter Tsvetkov[d], George Georgiou[e,f], Candice Lamb[f], Everett Stone[e], Pere Puigserver[b,c,d], Carmen Priolo[a,1,2], and Elizabeth P. Henske[a,1,2]

Edited by Tak Mak, University of Toronto, Toronto, Canada; received December 17, 2021; accepted April 14, 2022

Chromophobe (Ch) renal cell carcinoma (RCC) arises from the intercalated cell in the distal nephron. There are no proven treatments for metastatic ChRCC. A distinguishing characteristic of ChRCC is strikingly high levels of reduced (GSH) and oxidized (GSSG) glutathione. Here, we demonstrate that ChRCC-derived cells exhibit higher sensitivity to ferroptotic inducers compared with clear-cell RCC. ChRCC-derived cells are critically dependent on cystine via the cystine/glutamate antiporter xCT to maintain high levels of glutathione, making them sensitive to inhibitors of cystine uptake and cyst(e)inase. Gamma-glutamyl transferase 1 (GGT1), a key enzyme in glutathione homeostasis, is markedly suppressed in ChRCC relative to normal kidney. Importantly, GGT1 overexpression inhibits the proliferation of ChRCC cells in vitro and in vivo, suppresses cystine uptake, and decreases levels of GSH and GSSG. Collectively, these data identify ferroptosis as a metabolic vulnerability in ChRCC, providing a potential avenue for targeted therapy for these distinctive tumors.

chromophobe renal cell carcinoma | gamma-glutamyl transferase 1 | ferroptosis | solute carrier family 7 member 11

Significance

Targeted therapeutic approaches for chromophobe renal cell carcinoma (ChRCC) are urgently needed. Here, we found that ChRCC is hypersensitive to ferroptosis induction via a mechanism that involves the gamma-glutamyl cycle. ChRCC can be therapeutically targeted by the inhibition of cystine uptake or treatment with cyst(e)inase in vitro and in vivo.

Chromophobe renal cell carcinoma (ChRCC) is the third most frequent type of RCC, representing around 5% of all kidney cancer (1–3). ChRCC is believed to arise from the specialized intercalated cells of the distal nephron (4, 5). ChRCCs are characterized by whole-chromosome losses—including chromosomes 1, 2, 6, 10, 13, 17, and 21 (6)—and a low mutational burden, with about 40% of cases in *The Cancer Genome Atlas* (TCGA) having no identifiable driver mutations (7). Tumor protein p53 is the most frequently mutated gene, with mutations in 32% of cases, followed by phosphatase and tensin homolog, with mutations in 9% of cases (7). Mutations in mechanistic target of rapamycin kinase (mTOR), neuroblastoma rat sarcoma proto-oncogene (NRAS), tuberous sclerosis complex 1 (TSC1), or TSC2 mutations are observed in around 23% of cases, collectively (7). In total, 18% of ChRCC tumors carry mutations in mitochondrially encoded electron transport chain complex I genes. The most frequently mutated gene is NADH oxidoreductase core subunit 5 (MT-ND5), and heteroplasmy rates in some tumors reach 70% or higher (7). Interestingly, ChRCC tumors exhibit accumulation of abnormal mitochondria and have the highest mitochondrial DNA copy number compared with clear-cell RCC (ccRCC) or papillary RCC and the highest expression levels for all mitochondrial DNA genes across 13 tumor types analyzed by the TCGA (8–10), suggesting that defects in mitochondrial metabolism may be critical to the pathogenesis of ChRCC. Despite these advances in our understanding of ChRCC, there are still no proven therapies for metastatic or unresectable tumors. Limited efficacy of mTOR inhibitors (e.g., everolimus), tyrosine kinase inhibitors (TKIs), and immune checkpoint inhibitors has been observed (11–13).

ChRCC tumors are characterized by reduced levels of γ-glutamyl amino acids and strikingly increased glutathione levels, both reduced (GSH) and oxidized (GSSG) forms, compared with normal kidney (14, 15). Gamma-glutamyl transferase 1 (GGT1) is a plasma membrane transpeptidase that cleaves extracellular glutathione, generating extracellular glutamate and cysteinyl-glycine to be imported as γ-glutamyl amino acids in the cell and feed glutathione synthesis. ChRCC tumors express extremely low levels of GGT1 (almost 100-fold less compared with normal kidney) and have increased expression of glutamate-cysteine ligase catalytic subunit (GCLC), glutathione synthetase, and solute carrier family 7 member 11 (SLC7A11) (14) as well as downregulation of GSH-degrading and -conjugating enzymes including *GGT5* and glutathione S-transferase (*GSTM2*, *GSTM3*) (15). These data suggest critical reprogramming of glutathione homeostasis in ChRCC.

Author affiliations: [a]Pulmonary and Critical Care Medicine, Brigham and Women's Hospital, Harvard Medical School, Boston, MA 02115; [b]Department of Cancer Biology, Dana-Farber Cancer Institute, Boston, MA 02115; [c]Department of Cell Biology, Harvard Medical School, Boston, MA 02115; [d]Broad Institute of MIT and Harvard, Cambridge, MA 02139; [e]Department of Molecular Biosciences, University of Texas at Austin, Austin, TX 78712; and [f]Department of Chemical Engineering, University of Texas at Austin, Austin, TX 78712

Author contributions: L.Z., D.K., H.F., H.C.L., P.T., P.P., C.P., and E.P.H. designed research; L.Z., C.S.H., D.K., D.Y., H.F., M.A., and H.C.L. performed research; G.G., C.L., and E.S. contributed new reagents/analytic tools; L.Z., C.S.H., D.K., D.Y., H.F., M.A., Y.T., H.C.L., P.P., C.P., and E.P.H. analyzed data; and L.Z., D.K., H.F., C.P., and E.P.H. wrote the paper.

The authors declare no competing interest.

This article is a PNAS Direct Submission.

[1]C.P. and E.P.H. contributed equally to this work.

[2]To whom correspondence may be addressed. Email: carmen_priolo@dfci.harvard.edu or ehenske@bwh.harvard.edu.

This article contains supporting information online at http://www.pnas.org/lookup/suppl/doi:10.1073/pnas.2122840119/-/DCSupplemental.

Published July 8, 2022.

Ferroptosis is a distinct form of regulated cell death characterized by iron-mediated accumulation of lipid peroxides on the cellular membrane (16). Ferroptosis has been implicated in neurodegenerative diseases, acute and chronic kidney injury, and diabetes, and ferroptosis resistance is believed to contribute to tumorigenesis (17–19). Under physiological conditions, glutathione peroxidase 4 (GPX4) utilizes GSH to neutralize lipid peroxidation. Ferroptosis can be induced by inhibiting GPX4 (20, 21) or by limiting the supply of GSH to GPX4 (22). Cysteine is the rate-limiting substrate for the synthesis of GSH. Cystine uptake is mediated by the cystine/glutamate antiporter xCT (SLC7A11) (23). RSL3 (GPX4 inhibitor) and erastin (xCT inhibitor) inhibit tumor growth in vitro and in vivo (24, 25) and induce ferroptosis in certain tumor types (26, 27).

Here, we report evidence that ChRCC is highly sensitive to induction of ferroptotic cell death via targeting the cystine/glutamate antiporter xCT, and ChRCC cells are dependent on cystine uptake to preserve high glutathione content. We found that the markedly elevated levels of intracellular GSH in ChRCC-derived cells are GGT1 dependent, thereby impacting sensitivity to reactive oxygen species (ROS)-induced oxidative stress as well as their proliferation in vivo. Our findings suggest that induction of ferroptosis via cysteine deprivation could be a highly effective therapeutic strategy for ChRCC tumors, a tumor type for which effective treatments are urgently needed.

Results

Low GGT1 Expression Promotes the Proliferation of ChRCC Cells In Vivo and In Vitro by Maintaining High GSH Levels. We and others have demonstrated that glutathione levels are strikingly elevated in ChRCC, to levels that are 50- to 100-fold higher than matched normal kidney. These high levels of glutathione are accompanied by extremely low expression of GGT1, which degrades extracellular GSH and is 100-fold lower in ChRCC compared with normal kidney at the messenger RNA (mRNA) level (7, 14) and 70-fold lower at the protein level (28). Exogenous GGT1 was expressed at higher levels than normal kidney to test gain-of-function effects on ChRCC tumorigenesis (Fig. 1*A* and *SI Appendix*, Fig. S1*A*) (29). GGT1 expression in UOK276 cells caused a 50% decrease in subcutaneous tumor growth compared with enhanced green fluorescent protein (EGFP)-expressing control cells (Fig. 1*B*). More than 50% of the mice implanted with GGT1-expressing UOK276 cells survived up to 130 d, while no mice implanted with EGFP-expressing cells survived during the same period ($P = 0.01$; Fig. 1*C*).

GGT1 expression did not affect the proliferation of UOK276 cells in vitro at baseline conditions, but it sensitized cells to 100 μM H_2O_2, suppressing their proliferation by 50% compared with control cells ($P < 0.01$, Fig. 1*D*). This antiproliferative effect was prevented by supplementing the media with *N*-acetyl cysteine (NAC) (Fig. 1*E*). In dose–response experiments, we found that UOK276 cells expressing EGFP or GGT1 had an IC50 of 343 and 87 μM for H_2O_2, respectively (*SI Appendix*, Fig. S2). Similar results were obtained using tertiary-butylhydroperoxide (TBH), an inducer of oxidative stress (Fig. 1*F*). These data indicate that GGT1 inhibits the proliferation of UOK276 cells in an oxidative-stress-dependent manner.

To better understand the metabolic changes induced by expression of GGT1, we performed mass-spectrometry-based metabolomic analysis of UOK276 cells with expression of GGT1 compared with EGFP-expressing UOK276 cells. We detected over 200 metabolites, 26 of which were changed by at least 1.5-fold. GGT1 expression decreased reduced glutathione (GSH) levels by more than 70% ($P < 0.01$) and oxidized glutathione (GSSG) by more than 50% ($P < 0.05$) compared with the control cells (Fig. 1*G* and Dataset S1). Quantitatively, GGT1 expression decreased GSH concentration from 39 to 3.5 nmol/mg total protein ($P < 0.01$; Fig. 1*H*). GGT1 expression also increased ROS levels by 2-fold ($P < 0.0001$) in UOK276-expressing GGT1 compared with control cells. This effect was reversed by treatment with 1 mM NAC for 24 h ($P < 0.01$; Fig. 1*I*).

Similar results were obtained in HEK293T cells. GGT1 expression (*SI Appendix*, Fig. S3*A*) led to a significant decrease in intracellular GSH (>70%, $P < 0.01$) (*SI Appendix*, Fig. S3*B*), increased sensitivity to H_2O_2 (300 μM; *SI Appendix*, Fig. S3*C*) and TBH (25 μM; *SI Appendix*, Fig. S3*D*), and increased ROS levels ($P < 0.01$; *SI Appendix*, Fig. S3*E*) compared with EGFP control cells. These effects were reversed when cells were treated with NAC (1 mM, 24 h). Consistent with the in vitro results, subcutaneous tumors generated using UOK276 cells expressing GGT1 had lower GSH ($P < 0.05$) compared with EGFP-expressing tumors (Fig. 1*J*). These data indicate that GGT1 expression supports ChRCC glutathione metabolism in a ROS-dependent manner.

To determine the impact of GGT1 expression in UOK276 cells, we measured the activity of GGT, extracellular glutathione levels, and glutamate levels. GGT1-expressing UOK276 cells had significantly higher GGT1 activity than EGFP control cells (*SI Appendix*, Fig. S4*A*). Consistent with this result, GGT1 expression suppressed extracellular GSSG by about 80% ($P < 0.01$) (*SI Appendix*, Fig. S4*B*) and increased the extracellular glutamate concentration by 2.5-fold ($P < 0.0001$) (*SI Appendix*, Fig. S4*D*). Finally, UOK276 cells, which have very low GGT1 expression, showed higher extracellular GSSG ($P < 0.0001$) compared with ccRCC 786-O cells (*SI Appendix*, Fig. S4*C*).

Taken together, these data indicate that low GGT1 expression is associated with high levels of GSH and GSSG in ChRCC cells.

Cystine Uptake and Expression of GCLC and GPX4 are Low GGT1 Dependent in ChRCC. Cysteine is a rate-limiting substrate for the synthesis of glutathione (30) and can be incorporated by cells as gamma-glutamyl cysteine, a product of GGT function. Cysteine can also be generated by reduction of cystine. Cystine uptake is mediated by the cystine/glutamate antiporter xCT, which is encoded by SLC7A11. Expression of SLC7A11 is significantly higher in ChRCC compared with normal kidney (14). To determine the impact of impaired GGT1 on SLC7A11-mediated cystine uptake, fluorescein isothiocyanate (FITC)-labeled cystine was added to the culture media of UOK276 cells expressing GGT1 or control cells, and cystine uptake was measured by flow cytometry after 3 h. GGT1 expression and xCT inhibition by imidazole ketone erastin (IKE) suppressed cystine uptake by 40 and 80%, respectively (Fig. 1*K*).

To further investigate the mechanisms through which low GGT1 maintains high GSH levels, we tested the impact of modulating GGT1 on the expression of key enzymes involved in GSH metabolism in kidney cells. GCLC is one of the two subunits of glutamate-cysteine ligase (GCL), a heterodimeric enzyme that is critical for de novo GSH synthesis. In the TCGA dataset, *GCLC* mRNA level was 2-fold higher in ChRCC compared with normal kidney. This feature is unique to ChRCC, since *GCLC* mRNA was unchanged in ccRCC (14). Interestingly, Kang et al. reported that GCLC has a glutathione-independent, noncanonical role in the protection against ferroptosis by maintaining glutamate homeostasis under cystine starvation (30). Glutathione is utilized by GPX4 to detoxify lipid hydroperoxide and to protect

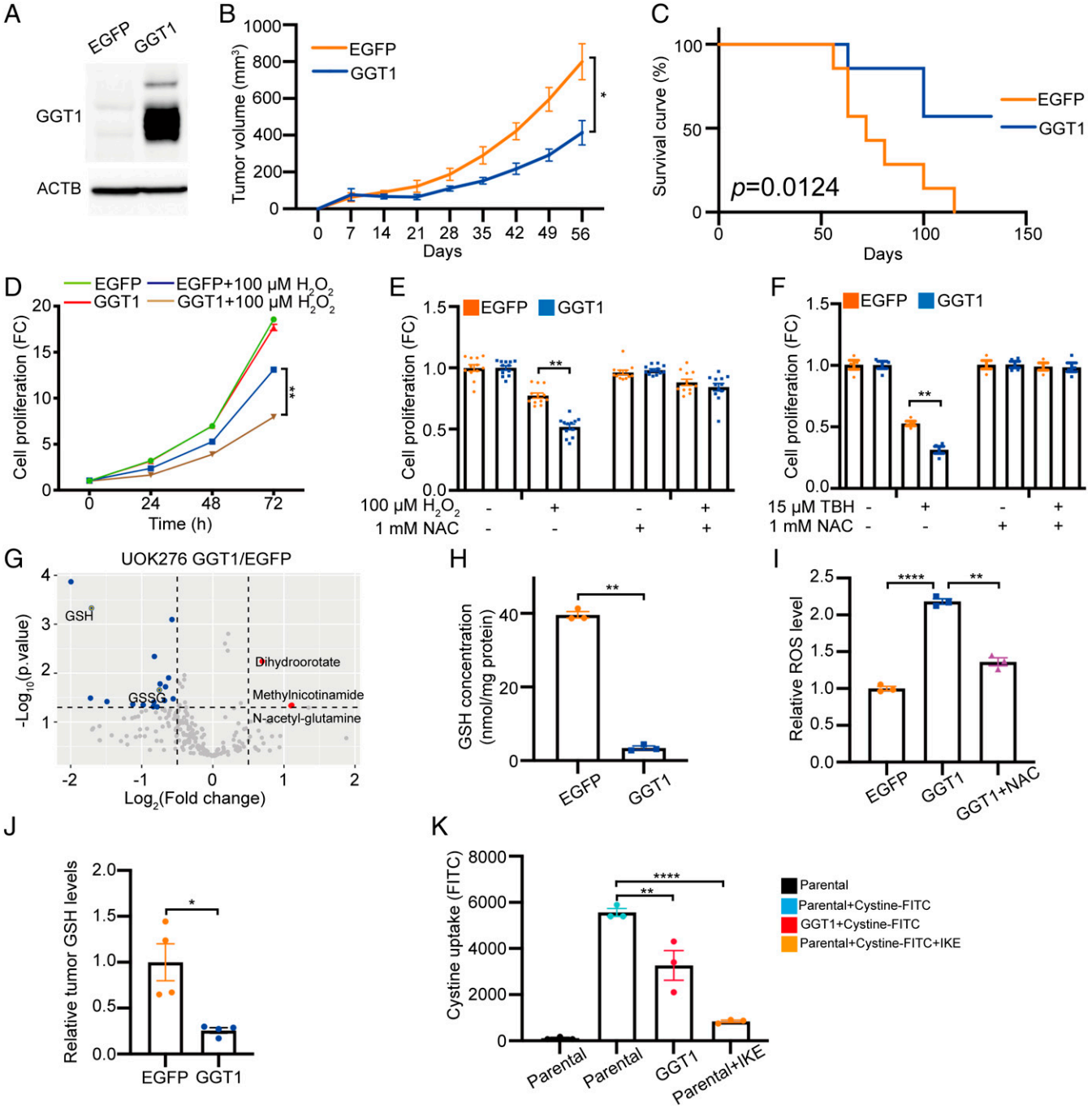

Fig. 1. Low GGT1 expression promotes the proliferation of ChRCC cells in vivo and in vitro by maintaining high GSH levels. (*A*) GGT1 protein levels in UOK276 cells expressing EGFP (control) or GGT1. (*B*) Tumor volume of EGFP- and GGT1-expressing UOK276 xenografts, $n = 6$ to 7 mice/group. (*C*) Survival curve for mice in *B* ($n = 6$ to 7 mice/group). (*D*) Proliferation (crystal violet) of UOK276 cells expressing EGFP or GGT1, with and without H_2O_2 (100 μM) treatment for 24, 48, and 72 h. (*E*) Proliferation (crystal violet) of UOK276 cells expressing EGFP or GGT1 treated with H_2O_2 (100 μM) or NAC (1 mM) alone or in combination for 48 h. (*F*) Proliferation (crystal violet) of UOK276 cells expressing EGFP or GGT1 treated with TBH (15 μM) or NAC (1 mM) alone or in combination for 48 h. (*G*) Volcano plot of differential metabolites in UOK276 cells with GGT1 expression compared with EGFP control ($n = 4$ biological replicates per condition). Blue signifies downregulation in GGT1-expressing cells, Red signifies upregulation. (*H*) GSH concentration in UOK276 cells with EGFP or GGT1 expression ($n = 3$ biological replicates per condition). (*I*) ROS level (Deep Red assay) in UOK276 cells with EGFP or GGT1 expression and with NAC (1 mM, 24 h) ($n = 3$ biological replicates per condition). (*J*) GSH concentration in EGFP- and GGT1-expressing UOK276 xenograft tumors shown in *B* ($n = 4$ biological replicates per condition). (*K*) Cystine-FITC (5 μM, 3 h) uptake in UOK276 cells with or without GGT1 expression, with or without IKE (1 μM, 3 h) treatment ($n = 3$ biological replicates per condition). Error bars represent mean ± SD. Statistical analyses were performed using two-tailed Student's *t* test or one-way ANOVA if more than two groups. $^*P < 0.05$; $^{**}P < 0.01$; $^{****}P < 0.0001$.

cells from ferroptosis (20). We found that *GPX4* mRNA levels were significantly higher in ChRCC tumors compared with normal kidney (TCGA data; Fig. 2*A*) and unchanged in ccRCC tumors (31) compared with normal kidney (Fig. 2*B*).

Consistent with these data from human tumors, GGT1 expression in UOK276 cells decreased *GCLC* and *GPX4* mRNA expression levels by more than 50% ($P < 0.01$; Fig. 2 *C* and *E*). Similarly, GGT1 expression in HEK293T cells reduced *GCLC* (50%, $P < 0.01$) and *GPX4* mRNA (60%, $P < 0.01$), while small interfering RNA (siRNA) knockdown of GGT1 in HEK293T cells increased *GCLC* and *GPX4* mRNA levels (Fig. 2 *C* and *E*). Protein levels of GCLC and GPX4 were also decreased in

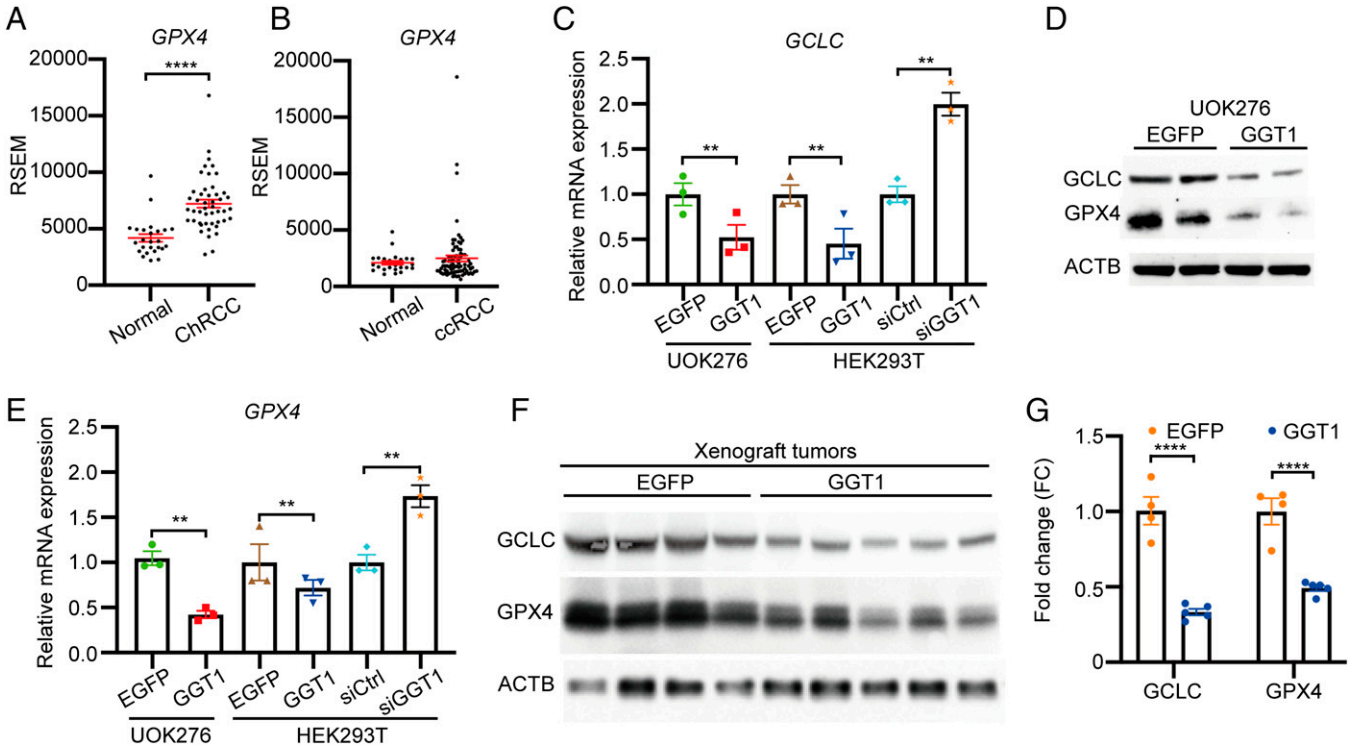

Fig. 2. Low GGT1 is associated with high expression of GCLC and GPX4 in ChRCC. (*A*) GPX4 mRNA level in ChRCC compared with normal kidney from TCGA. (*B*) GPX4 mRNA level in ccRCC compared with normal kidney from TCGA. (*C* and *E*) qRT-PCR analyses of GCLC (*C*) and GPX4 (*E*) expression in UOK276 and HEK293T cells with the indicated expression of EGFP or GGT1 or with siRNA for GGT1 ($n = 3$ biological replicates per condition). (*D* and *F*) GCLC and GPX4 protein expression in UOK276 cells with EGFP or GGT1 expression in vitro (*D*) and in vivo (*F*). (*G*) Quantitation of GCLC and GPX4 protein expression from *F* using Image J. Error bars represent mean ± SD. Statistical analyses were performed using two-tailed Student's *t* test or one-way ANOVA if more than two groups. $^{**}P < 0.01$; $^{****}P < 0.0001$.

GGT1-expressing UOK276 cells in vitro (Fig. 2*D*) and in vivo (Fig. 2 *F* and *G*).

Low GGT1 Expression Is Associated with Nuclear Accumulation of NRF2. NRF2 (also known as NFE2L2) is a transcription factor that plays an important role in the cellular response to oxidative stress and is known to promote GCLC and GPX4 expression (32, 33). To determine whether NRF2 plays a role in the regulation of glutathione synthesis in ChRCC, we downregulated this transcription factor in UOK276 cells using siRNA. NRF2 knockdown suppressed GCLC and GPX4 expression (Fig. 3*A*) and reduced GSH levels by 80% (Fig. 3*C*). Next, we assessed the nuclear localization of NRF2 in UOK276 cells expressing EGFP or GGT1. UOK276-EGFP cells had ∼50% ($P < 0.0001$) higher nuclear NRF2, as shown by immunofluorescence (Fig. 3*B*) and subcellular fractionation (Fig. 3*D*), compared with GGT1-expressing cells. Kelch-like golgi apparatus membrane protein-like protein ECHIDNA (ECH)-associated protein 1 (Keap1) is an oxygen sensor protein that downregulates NRF2 levels via proteasomal degradation (34, 35). Keap1 downregulation using siRNA (Fig. 3*E*) significantly enhanced both GCLC expression and GSH levels in UOK276-GGT1 and UOK276-EGFP control cells (Fig. 3 *F*, *I*, and *K*). Consistent with this result, KI-696, a small-molecule activator that disrupts Keap1-NRF2 binding, increased *GCLC* expression and GSH levels (Fig. 3 *G*, *J*, and *L*), suggesting that modulation of NRF2 participates in the regulation of glutathione synthesis in ChRCC cells.

Cystine Starvation Inhibits ChRCC Proliferation In Vitro and In Vivo. Inhibition of cystine uptake induces ferroptosis, and cystine starvation impairs cancer cell growth (30, 36). We found that UOK276 cells and ChromoA cells (derived from a ChRCC) (37) were more sensitive to cysteine starvation than 786-O cells. This phenotype was reversed by cotreatment with the ferroptosis inhibitor Ferrostatin-1 (Fer-1) (Fig. 4 *A* and *B*). Interestingly, based on TCGA data, SLC7A11 has higher expression in ChRCC compared with normal kidney but is not elevated in ccRCC (14). We generated two UOK276 lines with stable short hairpin RNA (shRNA)-driven knockdown of SLC7A11, achieving ∼80% knockdown efficiency (Fig. 4*C*). SLC7A11 downregulation inhibited the proliferation of UOK276 cells (Fig. 4*D*) in vitro. In vivo, downregulation of SLC7A11 inhibited the growth of UOK276 xenograft tumor volume and weight (Fig. 4 *E* and *F*).

Inhibition of the Cystine/Glutamate Antiporter xCT Reduces GSH Levels and Suppresses ChRCC Xenograft Tumor Growth. Since loss of GGT1 expression critically modulates GSH levels in UOK276 cells, we investigated whether this metabolic reprogramming generates a dependency with therapeutic implications for ChRCC. Interestingly, TBH-induced cell death was prevented by the ferroptosis inhibitor Fer-1 (1 μM) but not by the apoptosis inhibitor z-VAD-FMK (zVAD) (5 μM) or the necroptosis inhibitor necrostatin-1 (2 μM) at 48 h (Fig. 5*A*) in UOK276 cells. These data suggest that increased oxidative stress in ChRCC cells leads to ferroptotic cell death.

To address this hypothesis, we used three distinct methods to induce ferroptosis: pharmacologic inhibition of GPX4, restriction of cysteine/cystine uptake through xCT inhibition, and degradation of cysteine/cystine pool with cyst(e)inase. First, to determine the sensitivity of ChRCC cells to GPX4 inhibition, we used RSL3, a GPX4 inhibitor (20). We found that ChRCC-derived UOK276 and ChromoA cells were more sensitive to RSL3 than ccRCC-derived 786-O cells (IC_{50} = 4.2, 10.4, and 36.7 nM,

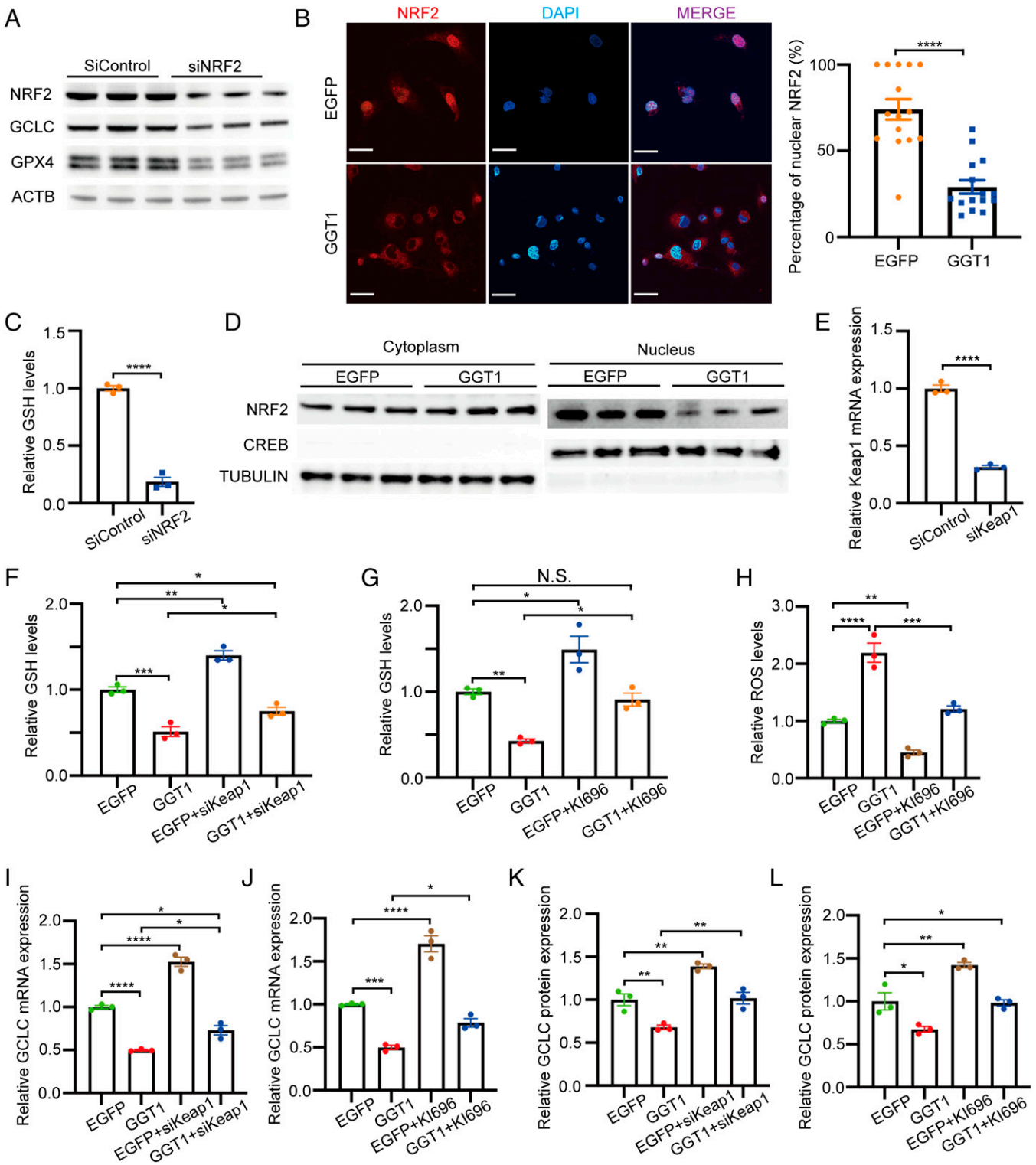

Fig. 3. Low GGT1 promotes GSH synthesis via NRF2-mediated GCLC expression. (*A*) GCLC and GPX4 protein expression in UOK276 cells with siRNA knockdown of NRF2 compared with control siRNA. (*B*) NRF2 immunofluorescence in UOK276 cells with EGFP or GGT1 expression and quantitation of nuclear localization by Image J. Scale bars: 30 μm (620×). (*C*) Relative GSH abundance in UOK276 cells with siNRF2 or siControl ($n = 3$ biological replicates per condition). (*D*) NRF2 protein expression in nuclear and cytoplasmic fractions of UOK276 cells with EGFP or GGT1 expression. (*E*) *Keap1* mRNA levels in UOK276 cells with siKeap1 or siControl ($n = 3$ biological replicates per condition). (*F*) Relative GSH abundance in UOK276 cells with GGT1 expression and siKeap1 or siControl ($n = 3$ biological replicates per condition). (*G*) Relative GSH abundance in UOK276 cells with GGT1 expression after 24-h treatment with KI696 or DMSO ($n = 3$ biological replicates per condition). (*H*) ROS levels (Deep Red assay) in UOK276 cells with EGFP or GGT1 expression after 24-h treatment with KI696 or DMSO ($n = 3$ biological replicates per condition). (*I*) *GCLC* mRNA levels in UOK276 cells with EGFP or GGT1 expression after 24-h treatment with KI696 or DMSO ($n = 3$ biological replicates per condition). (*J*) *GCLC* mRNA levels in UOK276 cells with EGFP or GGT1 expression and siKeap1 ($n = 3$ biological replicates per condition). (*K*) GCLC protein levels in UOK276 cells expressing EGFP or GGT1 after 24-h treatment with KI696 or DMSO. Densitometry was performed using Image J and GCLC/actin ratio calculated for three biological replicates per condition. (*L*) GCLC protein levels in UOK276 cells with EGFP or GGT1 expression and siKeap1. Densitometry was performed using Image J and GCLC/actin ratio calculated for three biological replicates per condition. Error bars represent mean ± SD. Statistical analyses were performed using two-tailed Student's *t* test or one-way ANOVA if more than two groups. $^{*}P < 0.05$; $^{**}P < 0.01$; $^{***}P < 0.001$; $^{****}P < 0.0001$.

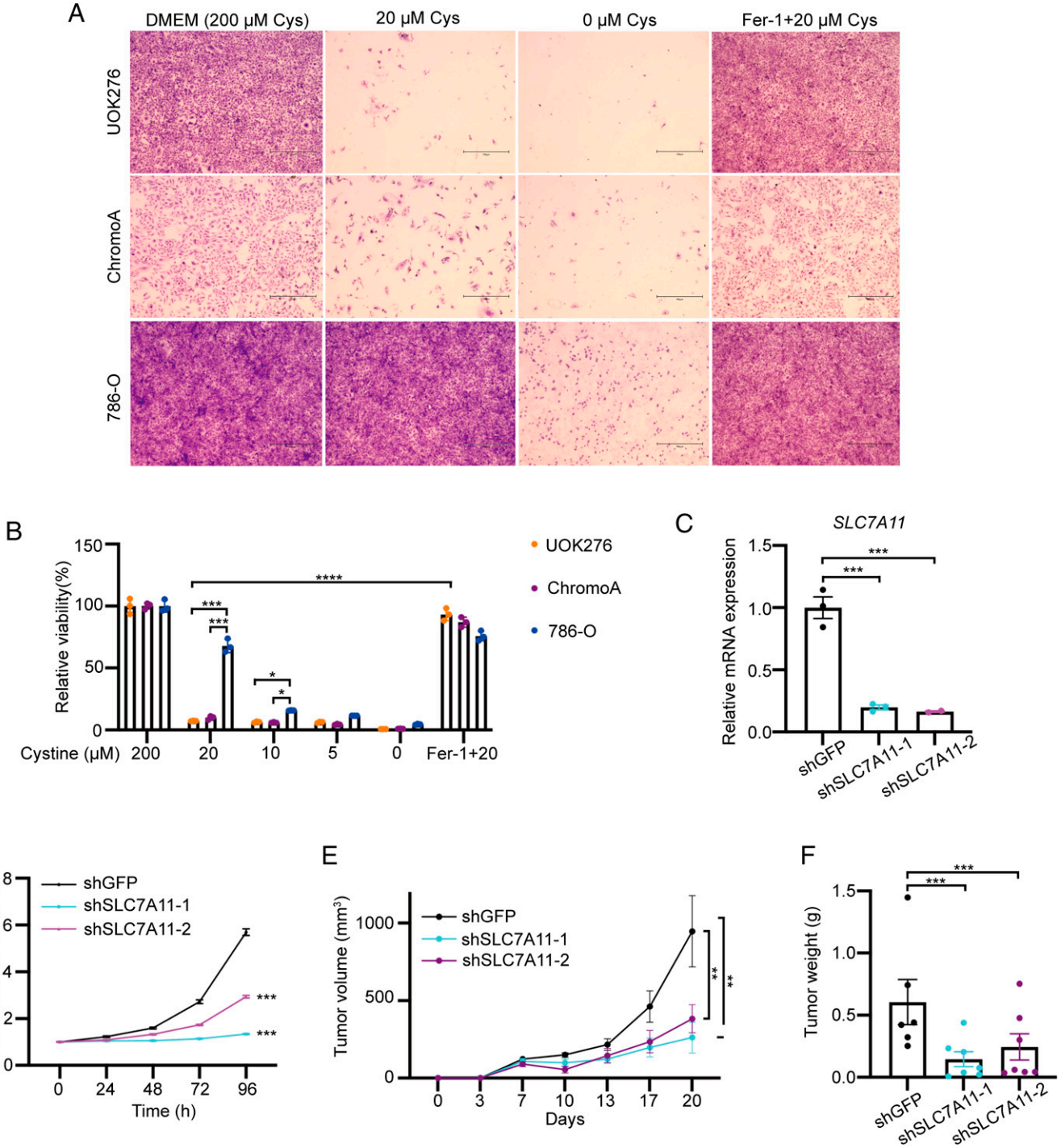

Fig. 4. Cystine starvation inhibits ChRCC proliferation in vitro and in vivo. (*A*) Representative images of crystal violet stained UOK276, ChromoA, and 786-0 cells grown for 48 h in DMEM versus cysteine-free media verus cysteine-free media supplemented with 20 μM cysteine with and without Fer-1 (1 μM), as indicated (n = 3 biological replicates per condition). Scale bars: 500 μm (40× magnification). (*B*) Relative cell viability of UOK276, ChromoA, and 786-0 cells grown for 48 h in DMEM versus cysteine-free media versus cysteine-free media supplemented with 5, 10, or 20 μM cysteine with and without Fer-1 (1 μM), measured by Cell Titer Glo (n = 3 biological replicates per condition). (*C*) SLC7A11 mRNA levels in UOK276 cells with knockdown of SLC7A11 using two different shRNAs (n = 3 biological replicates per condition). (*D*) Proliferation (crystal violet) of UOK276 cells with shRNA knockdown of SLC7A11 (n = 32 biological replicates per condition). (*E*) Tumor volume of UOK276 xenograft tumors expressing control (GFP) and SLC7A11 shRNAs. (*F*) Tumor weight of UOK276 xenograft tumors expressing control (GFP) and SLC7A11 shRNAs at day 21 (n = 6 to 7 mice/group). Error bars represent mean ± SD. Statistical significance was calculated using one way ANOVA with Tukey's multiple comparisons test. $^{**}P < 0.01$; $^{***}P < 0.001$; $^{****}P < 0.0001$.

respectively) (Fig. 5*B*). These results are of particular interest since in prior work, ccRCC was found to be highly sensitive to GPX4 inhibition via a HIF-2alpha-dependent mechanism (38), and our data indicate that ChRCC cells are even more sensitive to RSL3 than 786-0 cells. Next, we tested the sensitivity of ChRCC cells to inhibition of cystine uptake. IKE is an erastin analog with higher potency and metabolic stability (24, 39) compared with erastin (16). IKE and erastin inhibit the cystine/cysteine transporter xCT, resulting in reduced GSH synthesis. UOK276 and ChromoA cells were also more sensitive to IKE than 786-O cells (IC_{50} = 0.4, 6.2, and 34.3 μM, respectively) (Fig. 5*C*). Finally, to determine the importance of

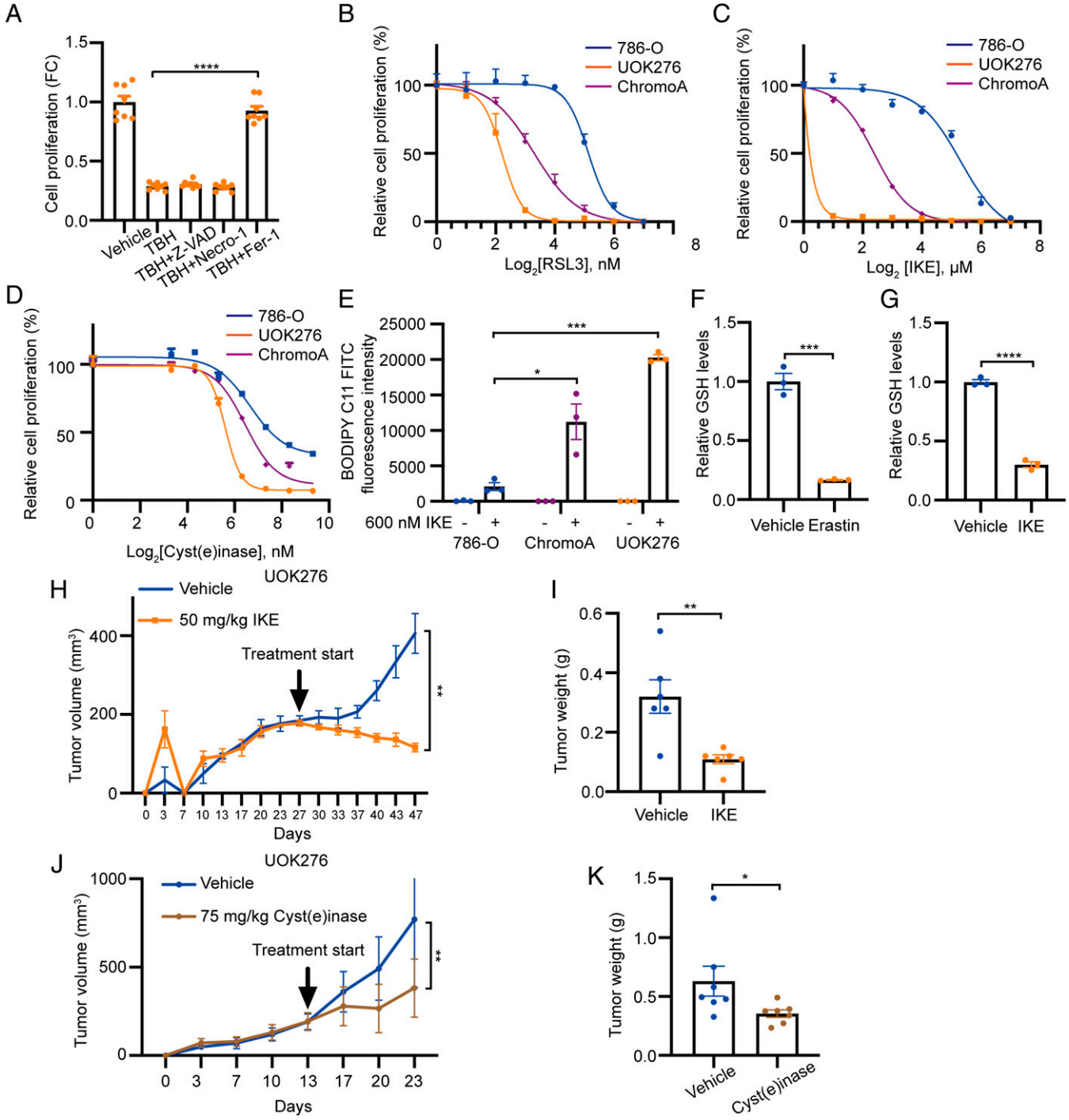

Fig. 5. Inhibition of cysteine/cystine-xCT axis reduces GSH levels and suppresses ChRCC xenograft tumor growth. (*A*) Proliferation (crystal violet) of UOK276 cells with EGFP or GGT1 expression treated with TBH (15 μM) alone or in combination with Fer-1 (1 μM), Z-VAD (5 μM), or necrostatin-1 (2 μM) for 48 h ($n = 8$ biological replicates per condition). (*B–D*) Proliferation (crystal violet) of 786-0, ChromoA, and UOK276 cells following 48-h treatment with RLS3 (*B*), IKE (*C*), or cyst(e)inase (*D*) at multiple concentrations ($n = 12$ biological replicates per condition). (*E*) Lipid peroxidation assessed by flow cytometry for BODIPY C11 in UOK276, ChromoA, and 786-0 cells after treatment with 600 nM IKE ($n = 3$ biological replicates per condition). (*F* and *G*) GSH levels in UOK276 cells after 24 h of 10 μM erastin (*F*) or 50 nM IKE (*G*) ($n = 3$ biological replicates per condition). (*H*) UOK276 xenograft tumor volume after treatment with IKE (50 mg/kg/day daily intraperitoneal) or vehicle control, beginning on day 28 ($n = 6$ to 7 mice/group). (*I*) UOK276 xenograft tumor weight on day 19 of vehicle and IKE treatment ($n = 6$ to 7 mice/group. (*J*) UOK276 xenograft tumor volume after treatment with vehicle or cyst(e)inase (75 mg/kg/day) ($n = 7$ mice/group). (*K*) Tumor weight at day 10 of cyst(e)inase treatment ($n = 7$ mice/group). Error bars represent mean ± SD. Statistical significance was calculated using one-way ANOVA with Tukey's multiple comparisons test. *$P < 0.05$; **$P < 0.01$; ***$P < 0.001$; ****$P < 0.0001$.

cysteine/cystine availability for ferroptosis in ChRCC, we used cyst(e)inase, an engineered and pharmacologically optimized human cyst(e)inase enzyme that depletes extracellular cysteine/cystine (26, 30). Both ChRCC cell lines, UOK276 and ChromoA, were more sensitive to cyst(e)inase treatment compared with 786-O cells (IC_{50}= 55.7, 84.4, and 147.0 nM, respectively) (Fig. 5*D*). Levels of lipid peroxidation (a marker of ferroptosis) after IKE treatment, assessed by BODIPY C11 staining and flow cytometry, were much higher in UOK276 and ChromoA cells than in 786-O cells (Fig. 5*E*). As expected, both erastin and IKE treatment led to a 70% ($P < 0.001$) decrease of intracellular GSH (Fig. 5 *F* and *G*). Treatment of mice bearing UOK276

tumors with IKE (50 mg/kg, daily) reduced tumor volume and tumor weight (Fig. 5 *H* and *I*) with no evidence of weight loss. This increased sensitivity of UOK276 cells to erastin and IKE treatment supports the translational hypothesis that ChRCC cells are dependent on cysteine/cystine uptake for their survival.

To further test this hypothesis, we used cyst(e)inase, which depletes the cysteine/cystine pools (26) and thereby induces ferroptosis (26, 30, 40, 41). We treated mice bearing UOK276 xenograft tumors for 10 d with 75 mg/kg cyst(e)inase ($n = 7$ per group). Cyst(e)inase suppressed tumor growth by ∼50% ($P < 0.01$), with no evidence of weight loss or systemic toxicity (Fig. 5 *J* and *K*). Together, these data demonstrate targeting glutathione metabolism by blocking cysteine availability induces ferroptosis in ChRCC cells.

Discussion

ChRCC is a rare kidney cancer subtype for which targeted therapy is not currently available. ChRCC is morphologically related to other renal neoplasms, including benign renal oncocytomas (42) and hybrid chromophobe oncocytic RCC (HOCT), which can occur in TSC and Birt-Hogg-Dube (BHD) syndromes (43). Many features of ChRCC distinguish it from ccRCC (the most common RCC subtype), including the nephron segment of origin (ChRCC arises from the intercalated cell in the distal nephron, which arises from the ureteric bud), the mutational profile (ChRCC lacks the von Hippel–Lindau tumor suppressor gene mutations that are the hallmark of ccRCC), and the karyotype (ChRCC has loss of multiple whole chromosomes). In contrast to the many major advances in the therapy of ccRCC—including TKIs, immunotherapy, and, most recently, combinations of TKI and immunotherapy (12)—there are currently no proven therapies for metastatic or unresectable ChRCC, and agents that are highly effective in ccRCC have, in general, shown little benefit in ChRCC (44–50).

Here, we first focused on the role of low GGT1 expression levels (a hallmark of ChRCC) (14, 15) in tumor pathogenesis. Physiologically, GGT1 degrades extracellular GSH to recycle its precursors for intracellular de novo GSH biosynthesis. In ccRCC, GGT1 is markedly upregulated, and downregulation of GGT1 decreases cell proliferation (51). A paradoxical role for GGT1, leading to increased consumption of GSH via a variety of mechanisms that include increasing the production of ROS, has also been proposed (52, 53). We found that low GGT1 in ChRCC-derived cells leads to the maintenance of high levels of intracellular GSH, creating a metabolic dependency to enhance resistance to oxidative stress and promote cell growth in vitro and in vivo.

Intriguingly, the mechanism of oxidative-stress-mediated cell death in UOK276 cells involves ferroptosis. The term ferroptosis was coined in 2012 to describe an iron-dependent regulated form of nonapoptotic cell death that most often results from oxidative stress and oxidation of long-chain polyunsaturated fatty acids in the plasma membrane (16).

These data led us to focus in more detail on the high levels of GSH that are a hallmark of ChRCC and, in particular, on cysteine, which is required for GSH synthesis. We found that ChRCC cell lines UOK276 and ChromoA cells are markedly more sensitive to the cystine uptake inhibitor, IKE, and to cyst(e)inase, when compared with ccRCC-derived 786-0 cells. IKE and cyst(e)inase treatment decreased the growth of UOK276 tumors in vivo by ∼60 and 30%, respectively. Knockdown of SLC7A11 also decreased the growth of ChRCC cells in vitro and in vivo.

Taken together, these data point toward a model in which ChRCC cells are highly dependent on cystine uptake in order to maintain their high levels of GSH (Fig. 6 *A* and *B*). Targeting cysteine availability, either by blocking cystine uptake (IKE) or promoting cysteine degradation with cyst(e)inase, may represent the first opportunities for targeted therapy for metastatic ChRCC. We hypothesize that this high demand for GSH biosynthesis may arise from the abundant abnormal mitochondria that are another hallmark of ChRCC (7, 10). These abnormal mitochondria have been historically observed by transmission electron microscopy (54). More recently, pan-TCGA analyses have revealed that ChRCC has the highest expression of the 13 mitochondrial DNA genes across several TCGA tumor types (10). It was recently discovered that ethidium bromide depletion of mitochondria in UOK276 cells leads to a 2-fold increase in GSH, suggesting that mitochondrial ROS may lead to high GSH utilization in ChRCC (15). Interestingly, benign renal oncocytomas, tumors that resemble ChRCC and have mitochondrial abnormalities (55), also have markedly elevated levels of GSH, up to 192-fold higher than matched normal kidney (14, 42). Chromophobe-like tumors termed HOCTs occur in two inherited syndromes, BHD and TSC (56–58), both of which are associated with mitochondrial dysregulation. Peroxisome proliferator activated receptor gamma coactivator 1 alpha (Pgc1a), which regulates mitochondrial biogenesis, is upregulated in BHD, and multiple defects in mitochondria have been discovered in TSC2-deficient cells and tumors (59). Loss of TSC2 and other mTOR pathway mutations has recently been shown to be linked to ferroptosis via ATF4 and SLC7A11 (60–63). Taken together, these data point toward a fundamental connection among ChRCC, oncocytomas, and HOCT and perhaps other tumors such as low-grade oncocytic tumor (64).

ChRCC, as well as oncocytomas and HOCT, originate from the intercalated cell in the distal nephron (5, 65). The distal nephron arises from the ureteric bud and plays critical roles in sodium balance via the principal cells and acid-base homeostasis via the intercalated cells. Intercalated cells have abundant membrane-localized V-ATPase, which drives hydrogen ion secretion into the urinary space, and are one of the most mitochondria-rich cells in the entire kidney, presumably because of the energetic requirements of the V-ATPase (66). We speculate that this mitochondrial abundance in intercalated cells causes a fundamental susceptibility to mitochondrial-driven oxidative stress, creating a "vicious cycle" of mitochondrial damage leading to increased ROS; leading to more mitochondrial damage; and thereby inducing tumors including oncocytomas, HOCT, and ChRCC. Importantly, from a translational perspective, this need for high GSH biosynthesis to neutralize ROS creates a dependence on cysteine that can be therapeutically targeted.

Novel therapeutic agents and clinical trials are urgently needed for ChRCC (67). Clinical trials have shown less efficacy of TKIs (68), mTOR inhibitors (11, 12), and immunotherapy (69) in metastatic ChRCC compared with ccRCC (44–50). The combination of everolimus (targeting mTOR) and Lenvatinib (targeting the vascular endothelial growth factor A receptors) has yielded the most promising results so far, with 9/15 partial responses in a single-arm phase II trial of nonclear-cell carcinoma (12). Since both mTOR inhibition and HIF2 alpha inhibition have been shown to induce ferroptosis (70, 71), it is possible that the benefit of the everolimus/Lenvatinib combination is related to GSH homeostasis.

In summary, we have discovered that ChRCC-derived cells are hypersensitive to ferroptotic cell death upon cysteine depletion. ChRCC-derived cells are more sensitive than ccRCC-derived cells

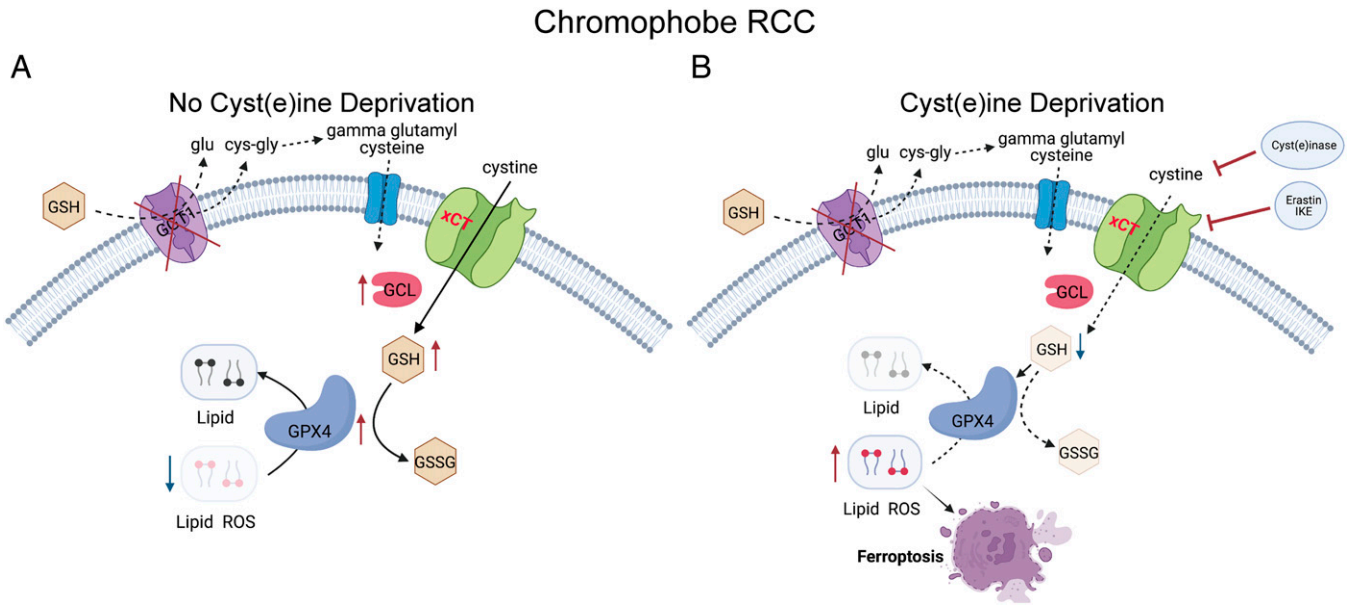

Fig. 6. Schematic diagram showing the mechanism underlying ChRCC sensitivity to ferroptosis. (*A*) ChRCC cells enhance cystine uptake and GCLC expression to synthesize glutathione (GSH). GPX4 utilizes GSH to neutralize lipid ROS and prevent ferroptosis. (*B*) Cystine deprivation by cyst(e)inase, erastin, or IKE suppresses GSH synthesis, leading to accumulation of lipid ROS and ferroptotic cell death. Dashed arrows indicate defective pathways. Glu, glutamate; Cys-gly, cysteinylglycine.

to the xCT inhibitor IKE, which is striking because ccRCC is known to be highly sensitive to ferroptosis induction (72). These data support the hypothesis that ChRCC cells are subject to high levels of oxidative stress in part because of their abundant and abnormal mitochondria, resulting in a dependence on cysteine/cystine to maintain adequate GSH levels and creating a targetable metabolic vulnerability.

Materials and Methods

Cell Lines and Culture Conditions. UOK276 cells were provided by Marston Linehan at the National Cancer Institute (29). HEK293T and 786-O cells were purchased from American Type Culture Collection (Manassas, VA). ChromoA (37) cells were obtained from Dr. Helmut Erich Gabbert at the University hospital of Düsseldorf. All cells were cultured in Dulbecco's modified Eagle medium (DMEM) containing 4.5 g/l glucose supplemented with 10% fetal bovine serum (FBS), 100 μg/mL penicillin, and 100 μg/mL streptomycin at 37 °C in a humidified incubator in an atmosphere of 5% CO_2.

Animal Studies. All animal studies were performed in accordance with protocols approved by the Brigham and Woman's Hospital Institutional Animal Care and Use Committee. The 6- to 7-wk-old athymic nude mice were injected subcutaneously in the left flank with 3.5 million UOK276 cells for IKE treatment or 5 million UOK276 cells for cyst(e)inase treatment. Tumor size was measured by electronic caliper twice per week and calculated using the formula 0.5 × length × width^2 until tumor size reached 1,000 mm^3, when mice were humanely euthanized. For IKE treatment, when tumors reached a volume of 200 ± 50 mm^3, mice were randomly separated into two groups: 1) vehicle group (daily intraperitoneal 65% D5W [5% dextrose in water], 5% Tween-80, 30% PEG-4000) and 2) IKE group (daily intraperitoneal 50 mg/kg IKE dissolved in 65% D5W [5% dextrose in water], 5% Tween-80, 30% PEG-4000). Each group consisted of six or seven mice that were treated for 19 d. For cyst(e)inase treatment, when tumors reached a volume of 200 ± 50 mm^3, mice were randomly separated into two groups: 1) vehicle group (phosphate buffered saline, PBS) and 2) cyst(e)inase group (daily intraperitoneal 75 mg/kg cyst(e)inase dissolved in Dulbecco's PBS with 10% glycerol). Each group consisted of seven mice that were treated for 10 d.

Metabolomic Profiling. Metabolites were processed using selected reaction monitoring with polarity switching on a 5500 quadropule ion trap (QTRAP) triple quadrupole mass spectrometer (AB/SCIEX) coupled to a Prominence ultra fast liquid chromatography (UFLC) high-performance liquid chromatography (HPLC) system (Shimadzu) using amide hydrophilic interaction chromatography (HILIC) chromatography (Waters) at pH 9.2 (Metabolomics Core, Beth Israel Deaconess Medical Center, Boston, MA). In total, 252 endogenous water-soluble metabolites were measured. Metabolomic peak area data were normalized to protein concentration of three additional replicate plates and uploaded into MetaboAnalyst 4.0 (https://www.metaboanalyst.ca/MetaboAnalyst/) for subsequent processing and metabolite set enrichment analysis. In detail, data were filtered by interquartile range, and autoscaling was applied to normalize data by metabolite (mean centered and divided by the SD of each variable).

Statistical Analyses. Data were analyzed for statistical significance with Student's unpaired *t* test, and multiple comparisons were made with one-way and two-way ANOVAs with Tukey's multiple comparisons test. In vivo data are presented as the mean ± 95% CI, and in vitro studies are presented as the mean ± SD (GraphPad Prism version 9; GraphPad Software). Statistical significance was defined as $P < 0.05$.

Data Availability. All study data are included in the article and/or *SI Appendix*.

ACKNOWLEDGMENTS. This work is supported by NIH Grant 1R01CA216922 to E.P.H. and C.P., the Tuttle Family, the van Hecke Family, the Christelis Family, the Cohen/Levin Family, the Dana-Farber/Harvard Cancer Center Kidney Cancer Specialized Program of Research Excellence Grant P50 CA101942-17, the National Institute of Diabetes and Digestive and Kidney Diseases Grant K01 DK116819 to H.C.L., and the Department of Defense Grant KC200051 to P.P.

1. H. Moch, A. L. Cubilla, P. A. Humphrey, V. E. Reuter, T. M. Ulbright, The 2016 WHO classification of tumours of the urinary system and male genital organs-Part A: Renal, penile, and testicular tumours. *Eur. Urol.* **70**, 93–105 (2016).
2. L. Zhang, E. P. Henske, Chromophobe renal cell carcinoma: New genetic and metabolic insights. *Urol. Oncol.* **38**, 678–681 (2020).
3. S. Avulova *et al.*, Grading chromophobe renal cell carcinoma: Evidence for a four-tiered classification incorporating coagulative tumor necrosis. *Eur. Urol.* **79**, 225–231 (2021).
4. D. Lindgren *et al.*, Cell-type-specific gene programs of the normal human nephron define kidney cancer subtypes. *Cell Rep.* **20**, 1476–1489 (2017).
5. S. L. Skala *et al.*, Next-generation RNA sequencing-based biomarker characterization of chromophobe renal cell carcinoma and related oncocytic neoplasms. *Eur. Urol.* **78**, 63–74 (2020).
6. W. M. Linehan, C. J. Ricketts, The cancer genome atlas of renal cell carcinoma: Findings and clinical implications. *Nat. Rev. Urol.* **16**, 539–552 (2019).
7. C. F. Davis *et al.*; The Cancer Genome Atlas Research Network, The somatic genomic landscape of chromophobe renal cell carcinoma. *Cancer Cell* **26**, 319–330 (2014).

8. E. Reznik *et al.*, Mitochondrial DNA copy number variation across human cancers. *eLife* **5**, e10769 (2016).
9. E. Reznik, Q. Wang, K. La, N. Schultz, C. Sander, Mitochondrial respiratory gene expression is suppressed in many cancers. *eLife* **6**, e21592 (2017).
10. Y. Yuan *et al.*; PCAWG Consortium, Comprehensive molecular characterization of mitochondrial genomes in human cancers. *Nat. Genet.* **52**, 342–352 (2020).
11. M. H. Voss *et al.*, Treatment outcome with mTOR inhibitors for metastatic renal cell carcinoma with nonclear and sarcomatoid histologies. *Ann. Oncol.* **25**, 663–668 (2014).
12. T. E. Hutson *et al.*, A single-arm, multicenter, phase 2 study of Lenvatinib plus everolimus in patients with advanced non-clear cell renal cell carcinoma. *Eur. Urol.* **80**, 162–170 (2021).
13. K. Zarrabi, E. Walzer, M. Zibelman, Immune checkpoint inhibition in advanced non-clear cell renal cell carcinoma: Leveraging success from clear cell histology into new opportunities. *Cancers (Basel)* **13**, 3652 (2021).
14. C. Priolo *et al.*, Impairment of gamma-glutamyl transferase 1 activity in the metabolic pathogenesis of chromophobe renal cell carcinoma. *Proc. Natl. Acad. Sci. U.S.A.* **115**, E6274–E6282 (2018).
15. Y. Xiao *et al.*, Decreased mitochondrial DNA content drives OXPHOS dysregulation in chromophobe renal cell carcinoma. *Cancer Res.* **80**, 3830–3840 (2020).
16. S. J. Dixon *et al.*, Ferroptosis: An iron-dependent form of nonapoptotic cell death. *Cell* **149**, 1060–1072 (2012).
17. W. S. Hambright, R. S. Fonseca, L. Chen, R. Na, Q. Ran, Ablation of ferroptosis regulator glutathione peroxidase 4 in forebrain neurons promotes cognitive impairment and neurodegeneration. *Redox Biol.* **12**, 8–17 (2017).
18. H. Lee *et al.*, Energy-stress-mediated AMPK activation inhibits ferroptosis. *Nat. Cell Biol.* **22**, 225–234 (2020).
19. J. Zheng, M. Conrad, The metabolic underpinnings of ferroptosis. *Cell Metab.* **32**, 920–937 (2020).
20. W. S. Yang *et al.*, Regulation of ferroptotic cancer cell death by GPX4. *Cell* **156**, 317–331 (2014).
21. J. M. Ubellacker *et al.*, Lymph protects metastasizing melanoma cells from ferroptosis. *Nature* **585**, 113–118 (2020).
22. N. Henke *et al.*, The plasma membrane channel ORAI1 mediates detrimental calcium influx caused by endogenous oxidative stress. *Cell Death Dis.* **4**, e470 (2013).
23. V. Câmpean, J. Kricke, D. Ellison, F. C. Luft, S. Bachmann, Localization of thiazide-sensitive Na(+)-Cl(−) cotransport and associated gene products in mouse DCT. *Am. J. Physiol. Renal Physiol.* **281**, F1028–F1035 (2001).
24. Y. Zhang *et al.*, Imidazole ketone erastin induces ferroptosis and slows tumor growth in a mouse lymphoma model. *Cell Chem. Biol.* **26**, 623–633 (2019).
25. Y. Shibata, H. Yasui, K. Higashikawa, N. Miyamoto, Y. Kuge, Erastin, a ferroptosis-inducing agent, sensitized cancer cells to X-ray irradiation via glutathione starvation in vitro and in vivo. *PLoS One* **14**, e0225931 (2019).
26. M. A. Badgley *et al.*, Cysteine depletion induces pancreatic tumor ferroptosis in mice. *Science* **368**, 85–89 (2020).
27. J. Wu *et al.*, Intercellular interaction dictates cancer cell ferroptosis via NF2-YAP signalling. *Nature* **572**, 402–406 (2019).
28. Y. Xiao *et al.*, Endocytosis-mediated replenishment of amino acids favors cancer cell proliferation and survival in chromophobe renal cell carcinoma. *Cancer Res.* **80**, 5491–5501 (2020).
29. Y. Yang *et al.*, Genomic and metabolic characterization of a chromophobe renal cell carcinoma cell line model (UOK276). *Genes Chromosomes Cancer* **56**, 719–729 (2017).
30. Y. P. Kang *et al.*, Non-canonical glutamate-cysteine ligase activity protects against ferroptosis. *Cell Metab.* **33**, 174–189 (2021).
31. Cancer Genome Atlas Research Network, Comprehensive molecular characterization of clear cell renal cell carcinoma. *Nature* **499**, 43–49 (2013).
32. H. Dong *et al.*, Nrf2 inhibits ferroptosis and protects against acute lung injury due to intestinal ischemia reperfusion via regulating SLC7A11 and HO-1. *Aging (Albany NY)* **12**, 12943–12959 (2020).
33. A. Loboda, M. Damulewicz, E. Pyza, A. Jozkowicz, J. Dulak, Role of Nrf2/HO-1 system in development, oxidative stress response and diseases: An evolutionarily conserved mechanism. *Cell. Mol. Life Sci.* **73**, 3221–3247 (2016).
34. M. Yamamoto, T. W. Kensler, H. Motohashi, The KEAP1-NRF2 System: A thiol-based sensor-effector apparatus for maintaining redox homeostasis. *Physiol. Rev.* **98**, 1169–1203 (2018).
35. M. Rojo de la Vega, E. Chapman, D. D. Zhang, NRF2 and the hallmarks of cancer. *Cancer Cell* **34**, 21–43 (2018).
36. Z. Shi, N. Naowarojna, Z. Pan, Y. Zou, Multifaceted mechanisms mediating cystine starvation-induced ferroptosis. *Nat. Commun.* **12**, 4792 (2021).
37. C. D. Gerharz *et al.*, Establishment and characterization of two divergent cell lines derived from a human chromophobe renal cell carcinoma. *Am. J. Pathol.* **146**, 953–962 (1995).
38. T. K. Choueiri, W. G. Kaelin Jr., Targeting the HIF2-VEGF axis in renal cell carcinoma. *Nat. Med.* **26**, 1519–1530 (2020).
39. L. F. Ye *et al.*, Radiation-induced lipid peroxidation triggers ferroptosis and synergizes with ferroptosis inducers. *ACS Chem. Biol.* **15**, 469–484 (2020).
40. W. Wang *et al.*, $CD8^+$ T cells regulate tumour ferroptosis during cancer immunotherapy. *Nature* **569**, 270–274 (2019).
41. Y. Li *et al.*, Sorafenib induces mitochondrial dysfunction and exhibits synergistic effect with cysteine depletion by promoting HCC cells ferroptosis. *Biochem. Biophys. Res. Commun.* **534**, 877–884 (2021).
42. R. K. Gopal *et al.*, Early loss of mitochondrial complex I and rewiring of glutathione metabolism in renal oncocytoma. *Proc. Natl. Acad. Sci. U.S.A.* **115**, E6283–E6290 (2018).
43. E. P. Henske, K. M. Cornejo, C. L. Wu, Renal cell carcinoma in tuberous sclerosis complex. *Genes (Basel)* **12**, 1585 (2021).
44. J. L. Lee *et al.*, Multicenter phase II study of sunitinib in patients with non-clear cell renal cell carcinoma. *Ann. Oncol.* **23**, 2108–2114 (2012).
45. A. M. Molina *et al.*, Phase II trial of sunitinib in patients with metastatic non-clear cell renal cell carcinoma. *Invest. New Drugs* **30**, 335–340 (2012).
46. I. Tsimafeyeu *et al.*, Phase II, multicenter, uncontrolled trial of single-agent capecitabine in patients with non-clear cell metastatic renal cell carcinoma. *Am. J. Clin. Oncol.* **35**, 251–254 (2012).
47. S. M. Keefe *et al.*, Efficacy of the nanoparticle-drug conjugate CRLX101 in combination with bevacizumab in metastatic renal cell carcinoma: Results of an investigator-initiated phase I-IIa clinical trial. *Ann. Oncol.* **27**, 1579–1585 (2016).
48. N. M. Tannir *et al.*, Everolimus versus sunitinib prospective evaluation in metastatic non-clear cell renal cell carcinoma (ESPN): A randomized multicenter phase 2 trial. *Eur. Urol.* **69**, 866–874 (2016).
49. M. H. Voss *et al.*, Phase II trial and correlative genomic analysis of everolimus plus bevacizumab in advanced non-clear cell renal cell carcinoma. *J. Clin. Oncol.* **34**, 3846–3853 (2016).
50. L. Bergmann *et al.*, A randomized phase IIa trial with temsirolimus versus sunitinib in advanced non-clear cell renal cell carcinoma: An intergroup study of the CESAR Central European Society for Anticancer Drug Research-EWIV and the Interdisciplinary Working Group on Renal Cell Cancer (IAGN) of the German Cancer Society. *Oncol. Res. Treat.* **43**, 333–339 (2020).
51. A. Bansal *et al.*, Gamma-glutamyltransferase 1 promotes clear cell renal cell carcinoma initiation and progression. *Mol. Cancer Res.* **17**, 1881–1892 (2019).
52. A. Corti, E. Belcastro, S. Dominici, E. Maellaro, A. Pompella, The dark side of gamma-glutamyltransferase (GGT): Pathogenic effects of an 'antioxidant' enzyme. *Free Radic. Biol. Med.* **160**, 807–819 (2020).
53. J. Zhang *et al.*, Oridonin induces ferroptosis by inhibiting gamma-glutamyl cycle in TE1 cells. *Phytother. Res.* **35**, 494–503 (2021).
54. G. Biczo *et al.*, Mitochondrial dysfunction, through impaired autophagy, leads to endoplasmic reticulum stress, deregulated lipid metabolism, and pancreatitis in animal models. *Gastroenterology* **154**, 689–703 (2018).
55. S. Joshi *et al.*, The genomic landscape of renal oncocytoma identifies a metabolic barrier to tumorigenesis. *Cell Rep.* **13**, 1895–1908 (2015).
56. L. S. Schmidt, Birt-Hogg-Dubé syndrome: From gene discovery to molecularly targeted therapies. *Fam. Cancer* **12**, 357–364 (2013).
57. H. C. Lam *et al.*, Rapamycin-induced miR-21 promotes mitochondrial homeostasis and adaptation in mTORC1 activated cells. *Oncotarget* **8**, 64714–64727 (2017).
58. H. C. Lam *et al.*, p62/SQSTM1 cooperates with hyperactive mTORC1 to regulate glutathione production, maintain mitochondrial integrity, and promote tumorigenesis. *Cancer Res.* **77**, 3255–3267 (2017).
59. D. Ebrahimi-Fakhari *et al.*, Impaired mitochondrial dynamics and mitophagy in neuronal models of tuberous sclerosis complex. *Cell Rep.* **17**, 1053–1070 (2016).
60. M. E. Torrence *et al.*, The mTORC1-mediated activation of ATF4 promotes protein and glutathione synthesis downstream of growth signals. *eLife* **10**, e63326 (2021).
61. Y. Zhang, P. Koppula, B. Gan, Regulation of H2A ubiquitination and SLC7A11 expression by BAP1 and PRC1. *Cell Cycle* **18**, 773–783 (2019).
62. P. Koppula, Y. Zhang, J. Shi, W. Li, B. Gan, The glutamate/cystine antiporter SLC7A11/xCT enhances cancer cell dependency on glucose by exporting glutamate. *J. Biol. Chem.* **292**, 14240–14249 (2017).
63. G. Lei, L. Zhuang, B. Gan, mTORC1 and ferroptosis: Regulatory mechanisms and therapeutic potential. *BioEssays* **43**, e2100093 (2021).
64. O. Kravtsov *et al.*, Low-grade oncocytic tumor of kidney (CK7-Positive, CD117-Negative): Incidence in a single institutional experience with clinicopathological and molecular characteristics. *Hum. Pathol.* **114**, 9–18 (2021).
65. A. Roy, M. M. Al-bataineh, N. M. Pastor-Soler, Collecting duct intercalated cell function and regulation. *Clin. J. Am. Soc. Nephrol.* **10**, 305–324 (2015).
66. S. Ghazi *et al.*, Multiparametric imaging reveals that mitochondria-rich intercalated cells in the kidney collecting duct have a very high glycolytic capacity. *FASEB J.* **34**, 8510–8525 (2020).
67. K. Ito, Recent advances in the systemic treatment of metastatic non-clear cell renal cell carcinomas. *Int. J. Urol.* **26**, 868–877 (2019).
68. R. J. Motzer *et al.*, Treatment outcome and survival associated with metastatic renal cell carcinoma of non-clear-cell histology. *J. Clin. Oncol.* **20**, 2376–2381 (2002).
69. T. K. Choueiri *et al.*, PD-L1 expression in nonclear-cell renal cell carcinoma. *Ann. Oncol.* **25**, 2178–2184 (2014).
70. Y. Zhang *et al.*, mTORC1 couples cyst(e)ine availability with GPX4 protein synthesis and ferroptosis regulation. *Nat. Commun.* **12**, 1589 (2021).
71. H. Miess *et al.*, The glutathione redox system is essential to prevent ferroptosis caused by impaired lipid metabolism in clear cell renal cell carcinoma. *Oncogene* **37**, 5435–5450 (2018).
72. Y. Zou *et al.*, A GPX4-dependent cancer cell state underlies the clear-cell morphology and confers sensitivity to ferroptosis. *Nat. Commun.* **10**, 1617 (2019).